SPACE Conferences & Exposition
4-7 August 2014, San Diego, CA
AIAA/AAS Astrodynamics Specialist Conference

# Enhancing Relative Attitude and Trajectory Estimation for Autonomous Rendezvous Using Flash LIDAR

Jay W. McMahon*, Steven Gehly†, and Penina Axelrad‡

**Initial results of a study on the use of flash LIDAR for relative pose and trajectory estimation are presented. Analysis is conducted for distant approach phases where flash LIDAR measurements are processed with no information about the target body shape and attitude, and for close approach phases where the relative pose is estimated simultaneously with the relative trajectory. In both cases, very good relative navigation accuracy can be obtained with errors based on current flash LIDAR models. The distant navigation analysis considered the necessary frequency of flash LIDAR data needed for accurate solutions, the effect of ignoring the target shape, and the growth of the achieved errors in the case of sensor malfunction. The close approach results are focused on the implementation of a combination of the Optimal Linear Attitude and Translation Estimator (OLTAE) algorithm for processing feature based tracking into relative attitude and translation measurements, combined with an extended Kalman filter (EKF) for estimating the full 6-DOF relative dynamic state.**



## I. Introduction

Autonomous rendezvous and docking between satellites offers a cost-effective alternative to manned missions to repair and refuel satellites on orbit, and extends the range of such missions to regions of space such as GEO that were not previously feasible.[3] The central problem is estimation of the relative position and attitude (pose) between the two satellites. Many combinations of instruments could be mechanized to approach this problem. Classical methods use optical measurements, however these provide angles only measurements which suffer from scale invariance problems. Optical measurements also rely on the natural lighting conditions, which at a minimum increases the difficulty for processing the data to estimate the pose. Radar systems may be used to determine the relative range to supplement optical data, however they offer limited information for estimating the attitude states.

The use of flash Light Detection and Ranging (LIDAR) instruments allows features to be extracted from the target spacecraft, which can then be compared to a reference model to solve the relative pose problem. Thus LIDAR provides both range and attitude information from a single sensor which is not affected by poor lighting conditions. A flash LIDAR instrument has been demonstrated during Space Shuttle docking to the ISS.[2]

This paper explores attitude and trajectory estimation performance using Flash LIDAR for all phases of autonomous rendezvous and docking. The impacts on estimation performance due to observation interval and sensor quality, target vehicle dynamics and shape, and a priori state knowledge are assessed. We also investigate the sensitivity of information acquired to the specific approach trajectory flown. The goal of this study is to understand under what conditions Flash LIDAR can be used as the key sensor for robust navigation and attitude estimation in autonomous rendezvous and docking.

*Assistant Research Professor, Aerospace Engineering Sciences, University of Colorado at Boulder, 431 UCB, Boulder, CO, 80309. Senior Member, AIAA

†Graduate Research Assistant, Aerospace Engineering Sciences, University of Colorado at Boulder, 429 UCB, Boulder, CO, 80309

‡Department Chair, Aerospace Engineering Sciences, University of Colorado at Boulder, 429 UCB, Boulder, CO, 80309. AIAA Fellow.

The analysis is presented in two parts. First, the approach navigation is analyzed for the portion of the trajectory when no information about the target body's shape and attitude is assumed. Second, we look at the close approach phase where the relative pose and trajectory are solved simultaneously.

## II. Approach Navigation

Approach navigation begins when the chaser spacecraft can first directly observe the target spacecraft. Initially, it is important to accurately estimate the relative state on approach so that a safe rendezvous can be achieved. To illustrate the applicability of using flash LIDAR for this phase of a rendezvous mission, an artificial rendezvous scenario similar to an ISS approach (e.g. as discussed in Ref. 1) was created. For simplicity in this study, the chaser and the target spacecraft begin in concentric circular orbits. The target spacecraft is in a ISS-like orbit (circular at 6793.5 km radius), while the chaser spacecraft is in a slightly lower circular orbit, gaining ground on the target from behind/below. It is assumed that initial sensor acquisition occurs at 5 km (based on the STORRM experiment[2]) and at just over 1 km range, the relative orbit of the target is known with $3\sigma$ uncertainties of less than 50 m in position and 10 m/s in velocity. This study starts at this point in the rendezvous scenario.

The trajectory of interest for the final approach studied in detail here is then pictured in Fig. 1. The final approach is composed of two portions, denoted as leg 1 and leg 2. Leg 1 lasts for 30 minutes, and goes from just over 1 km down to 250 m range. Leg 2 then goes roughly along the r-bar down to a range of 20 m over 10 minutes. The range profile of this trajectory is shown in Fig. 2. Fig. 1 also includes the $3\sigma$ position uncertainties at each point after a measurement is taken, here assumed to be every 60 seconds. At this scale, the position uncertainties appear coincident with the target location.

The flash LIDAR is assumed to have a 256 x 256 pixel array with a total field of view of 20° on each side. The range measurements include Gaussian noise with a $3\sigma$ equal to 10 cm + 1% of the current range. The results presented in this section use the center-of-figure as the measurement in the filter. In other words, the location and range of all pixels with a return from the target are averaged together to produce a single relative position vector observation. This necessarily introduces error in the estimates, which is discussed below.

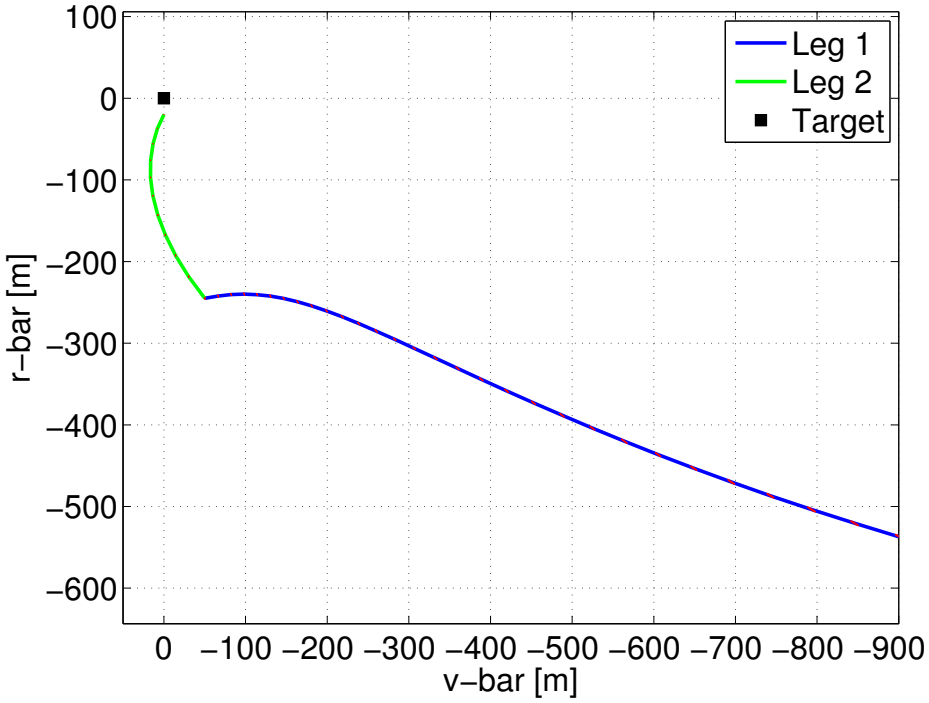


**Figure 1. Nominal final approach in the target radial/in-track plane with $3\sigma$ uncertainties (in red) for a measurement every 60 seconds. At this scale the uncertainties are within the line thickness.**

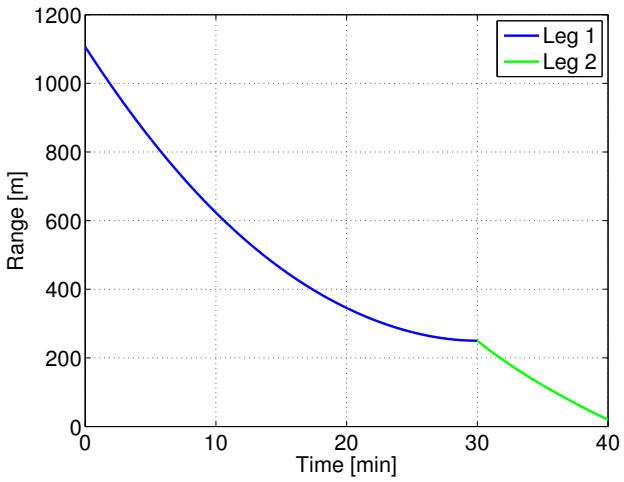


**Figure 2. Time history of range vs time over nominal final approach.**

The target spacecraft for this study is a simple box-and-wing model with dimensions similar to the Iridium spacecraft. The shape model and a simulated flash LIDAR "image" are shown in Fig. 3. Note the LIDAR image is flipped only due to the particular axis definitions used in the simulation.

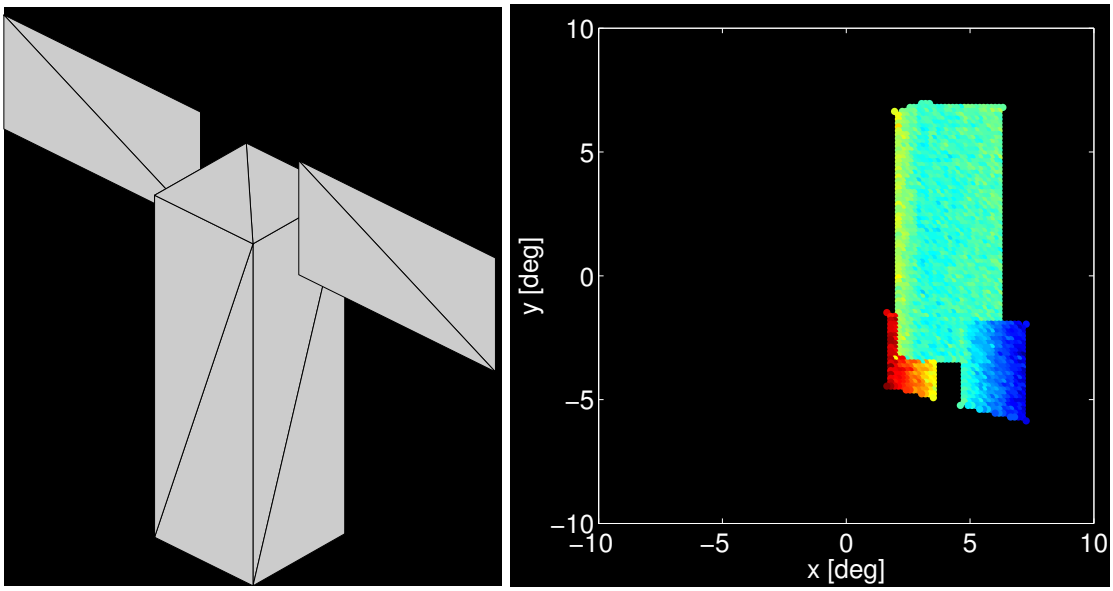


**Figure 3. Illustration of the target spacecraft shape model (left) and a simulated flash LIDAR image (right). Note the flash LIDAR image appears inverted due to the choice of the sensor frame coordinates.**

LIDAR range measurements are very accurate for approach navigation to 250 m. separation, and thus the knowledge based on these measurements is fairly high. The planar uncertainties when using measurements every 60 seconds are shown in Fig. 4. The uncertainty in the line-of-sight direction is driven by the noise on the measurements, while the errors in cross direction (defined to be in the orbit plane, perpendicular to the line-of-sight direction) are controlled by the flash LIDAR pixel resolution. Note that although the position estimates are very accurate, taking measurements at intervals of 60 seconds does not provide a lot of knowledge for the velocity states due to the fact that the velocities must be inferred through the dynamic evolution of the system; the measurements don't directly provide any velocity information. This issue can alleviated by taking more dense measurements, an example of which is illustrated in Fig. 5 where measurements are taken every second.

At this point it is clear that, under nominal conditions, a flash LIDAR provides plenty of information to accurately estimate the relative orbit state of a target spacecraft on final approach. Furthermore, this

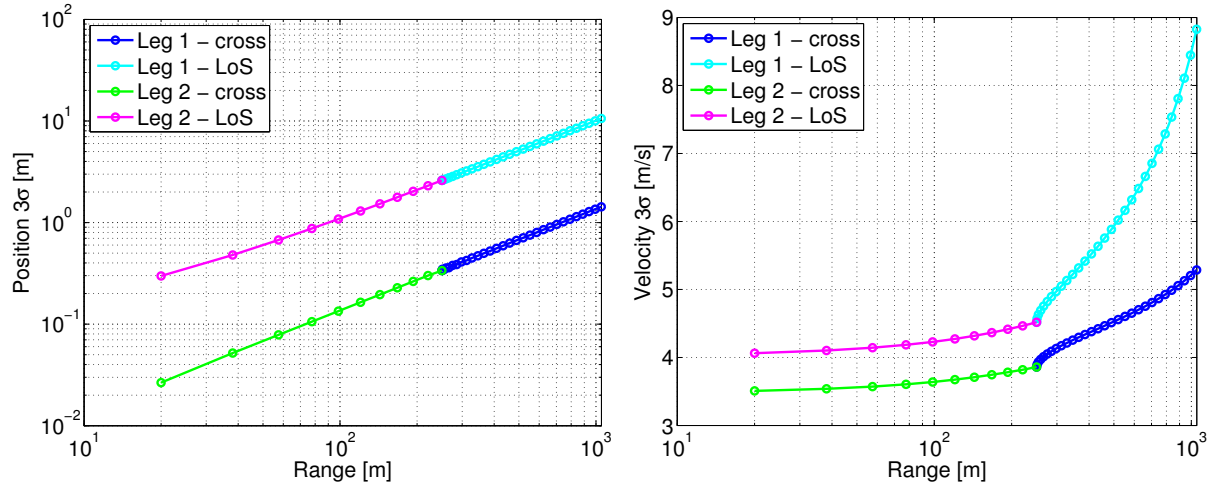


**Figure 4. Planar $3\sigma$ position and velocity uncertainties along the nominal trajectory with a measurement every 60 seconds. Uncertainties are reported in terms of the line-of-sight and perpendicular in-plane directions.**

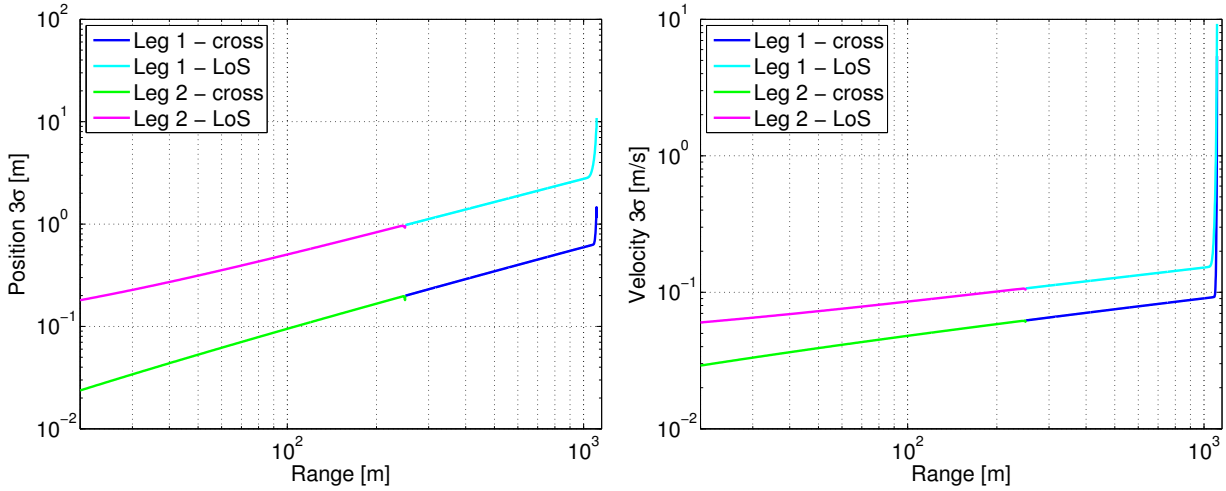


**Figure 5. Planar $3\sigma$ position and velocity uncertainties along the nominal trajectory with a measurement every 1 second. Uncertainties are reported in terms of the line-of-sight and perpendicular in-plane directions.**

can be done with minimal information about the shape of the target spacecraft. In fact, in the examples shown here no information about the target shape is used. As mentioned above, the filter assumes that the center-of-figure observed is actually the center-of-mass of the target. This is clearly incorrect - not only is there a range offset since the LIDAR observes the exterior of the spacecraft, but furthermore there will generally be angular errors as well due to the fact that spacecraft will not appear symmetrically with respect to the center-of-mass.

The errors induced from this assumption can be seen in Fig. 6. Most clearly, due to the asymmetric shape of the target model shown in Fig. 6, the errors appear as a nearly constant bias. The difference between the observed center-of-figure and the estimated center-of-mass are illustrated in Fig. 7. It can be seen that the filter moves its estimate of the center-of-mass to match the observed center-of-figure since it has no knowledge that these are not in fact the same.

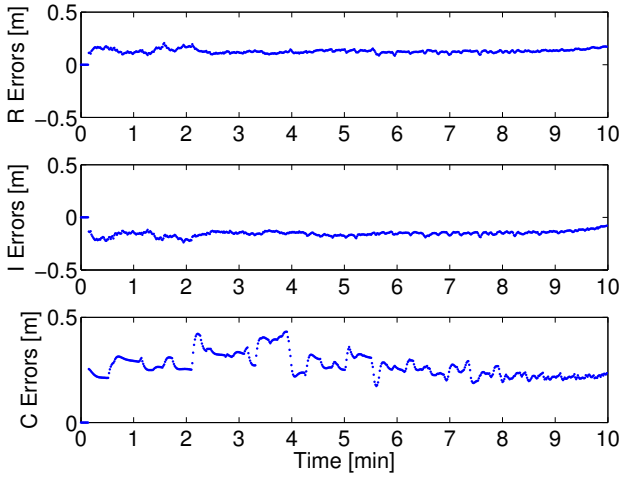


**Figure 6. LVLH position errors between the filter estimate and the truth for case using measurements at 1 Hz. Note the biases due to lack of shape model knowledge.**

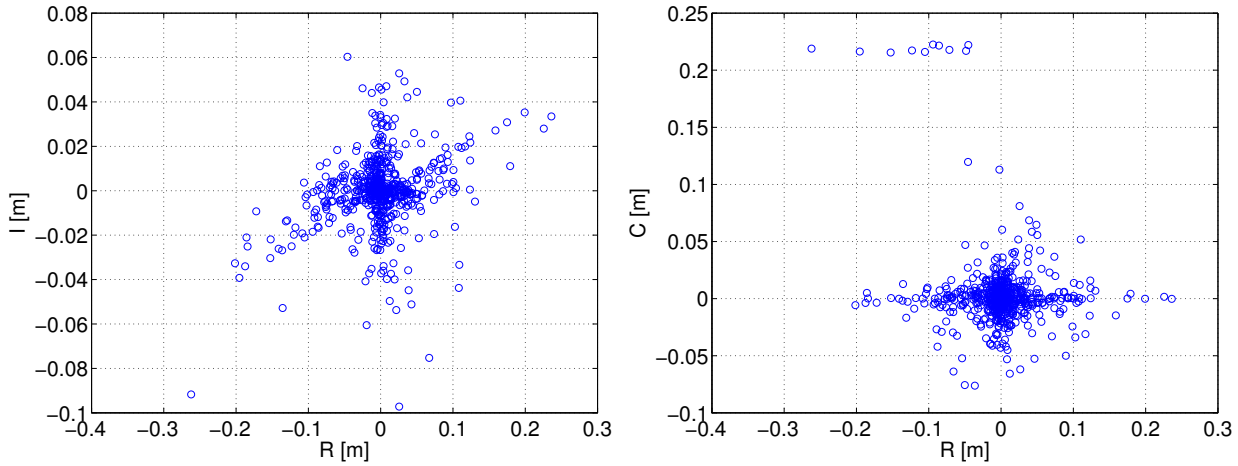


**Figure 7. Observed center-of-figure offsets from estimated center-of-mass.**

Finally, while under nominal conditions the flash LIDAR works well, it is important to understand the limits of the estimation accuracy. In Fig. 8 some initial analysis of the uncertainty propagation under sensor failure are shown. The left picture shows how the very small (at this scale) initial uncertainties quickly grow if no measurements are made at all on leg 2 of the final approach. This is due to the fact that velocity knowledge is limited when using this instrument. Although the 1 Hz measurement updates shown in Fig. 5 provide velocity knowledge on the order of 10 cm/s at the end of leg 1, this is large enough to cause the position uncertainty to grow rather rapidly under the natural dynamics of the system. It turns out, as shown

in the right of Fig. 8, that measurements need to be taken up to about 5 minutes before reaching the 20 m point (so down to a range of about 120 m) in order to keep the $3\sigma$ ellipsoid from intersecting the target.

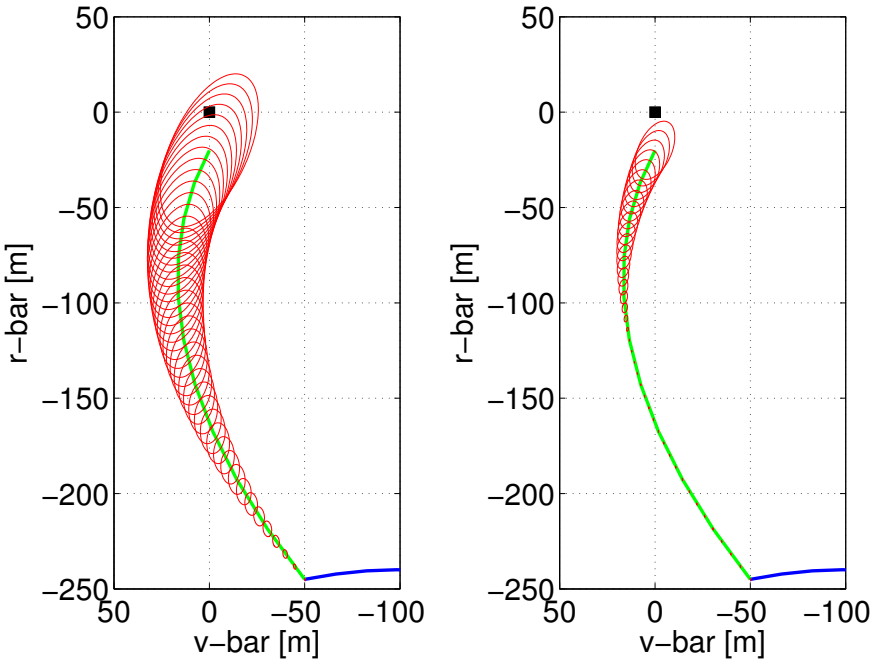


**Figure 8. Propagation of $3\sigma$ uncertainty for leg 2 assuming no measurements taken during leg 2 (left) or no measurements taken for the last 5 minutes of leg 2 (right).**

## III. Relative Pose Estimation

The more challenging problem is estimation of the relative position and attitude (pose) between the two satellites. The use of LIDAR instruments allows features to be extracted from the target spacecraft, which can then be compared to a reference model to solve the relative pose problem. LIDAR provides both range and angle measurements of the feature points, and is not affected by poor lighting conditions. In the following sections we review the OLTAE theory, and then present several simulations illustrating the use of OLTAE combined with an EKF to estimate the full relative state and pose.

### A. Estimation Theory

The method used to solve the relative pose problem in this paper is the Optimal Linear Attitude and Translation Estimator (OLTAE) developed by Junkins and co-authors,[9,6] which built upon the previous Optimal Linear Attitude Estimator (OLAE) theory.[10] Following the derivation presented by Flewelling in Reference 6, the relationship between the observed and reference points may be stated as

$$\boldsymbol{x}_i^* = C\boldsymbol{x}_i + \boldsymbol{T} + \boldsymbol{\epsilon} \tag{1}$$

where $\boldsymbol{x}_i^*$ is the position vector of an observed point in a sensor-defined frame, $\boldsymbol{x}_i$ is the position vector of the reference point in the target's body-fixed frame, $C$ represents the rotation between the two frames, $\boldsymbol{T}$ is the relative translation vector, and $\boldsymbol{\epsilon}$ is a zero mean white noise vector. The attitude states can be re-parameterized using the 3 component Gibbs vector, and the 6DOF relative pose problem solved using a linear least squares fit.

The Gibbs vector is defined by

$$\boldsymbol{g} = \hat{\boldsymbol{e}}\tan(\phi/2) \tag{2}$$

where $\hat{\boldsymbol{e}}$ is the principal rotation axis unit vector and $\phi$ is the angle of rotation. The Gibbs vector is related to the rotation matrix $R$ by the Cayley transform

$$C = [I + \tilde{\boldsymbol{g}}]^{-1}[I - \tilde{\boldsymbol{g}}] \tag{3}$$

where $\tilde{\boldsymbol{g}}$ indicates the skew symmetric matrix

$$\tilde{\boldsymbol{g}} = \begin{bmatrix} 0 & g_3 & -g_2 \\ -g_3 & 0 & g_1 \\ g_2 & -g_1 & 0 \end{bmatrix} \tag{4}$$

By substituting for $C$ in Eq. (1) and pre-multiplying by $[I + \tilde{\boldsymbol{g}}]$, the following relationship is obtained.

$$[I + \tilde{\boldsymbol{g}}]\boldsymbol{x}_i^* = [I - \tilde{\boldsymbol{g}}]\boldsymbol{x}_i + [I + \tilde{\boldsymbol{g}}]\boldsymbol{T} \tag{5}$$

Gathering terms and making use of the cross product property $[\tilde{\boldsymbol{a}}]\boldsymbol{b} = -[\tilde{\boldsymbol{b}}]\boldsymbol{a}$, the problem assumes the standard form $\boldsymbol{y} = H\boldsymbol{x}$.

$$\boldsymbol{x}_i^* - \boldsymbol{x}_i = [\tilde{\boldsymbol{x}}_i^*]\boldsymbol{g} + [\tilde{\boldsymbol{x}}_i]\boldsymbol{g} + [I + \tilde{\boldsymbol{g}}]\boldsymbol{T} \tag{6}$$

$$\boldsymbol{x}_i^* - \boldsymbol{x}_i = [\widetilde{\boldsymbol{x}_i^* + \boldsymbol{x}_i}]\boldsymbol{g} + \boldsymbol{T}^* \tag{7}$$

$$\boldsymbol{x}_{\text{diff},i} = [\widetilde{\boldsymbol{x}_{\text{sum},i}} \quad I_{3x3}] \begin{bmatrix} \boldsymbol{g} \\ \boldsymbol{T}^* \end{bmatrix} \tag{8}$$

where $\boldsymbol{T}^* = [I + \tilde{\boldsymbol{g}}]\boldsymbol{T}$ is a set of transformed position coordinates and the $\boldsymbol{y}$ and $H$ terms of Eq. (8) are shown for feature $i$ only. In the full problem using $N$ features, these terms will have dimension $3N \times 1$ and $3N \times 6$ respectively. Provided enough features are available, the problem is well posed and the $6 \times 1$ state vector $[\boldsymbol{g}^T \quad \boldsymbol{T}^{*T}]^T$ is observable. Additionally, it is noted that the Gibbs vector is a suitable choice for the attitude representation because the relationship in Eq. (8) is linear and therefore any resultant errors are due to measurement noise and not linearization.

In order to minimize the impact of measurement noise, a weighted least squares solution is obtained from

$$\hat{\boldsymbol{x}} = [H^T R^{-1} H]^{-1} H^T R^{-1} \boldsymbol{y} \tag{9}$$

$$P = [H^T R^{-1} H]^{-1} \tag{10}$$

where $\hat{\boldsymbol{x}} = [\hat{\boldsymbol{g}}^T \quad \hat{\boldsymbol{T}}^{*T}]^T$, $H = [\widetilde{x_{i,\text{sum}}} \quad I_{3x3}]$ is the $3Nx6$ observation mapping matrix, and $\boldsymbol{y} = [\boldsymbol{x}_i^* - \boldsymbol{x}_i]$ is the $3Nx1$ observation residual vector for all $N$ points. Note that the transformation back to the estimated position $\hat{\boldsymbol{T}}$ must be computed using the estimated values $\hat{\boldsymbol{g}}$ and $\hat{\boldsymbol{T}}^*$ by

$$\hat{\boldsymbol{T}} = [I + \tilde{\hat{\boldsymbol{g}}}]^{-1} \hat{\boldsymbol{T}}^* \tag{11}$$

To determine the correct measurement noise covariance $R$, it is necessary to consider the LIDAR measurement model in terms of the sensor LVLH frame. The LIDAR measurement to a feature point on the target is modeled using the range $\rho$ from the sensor's focal plane to the feature, and two angles $\alpha$ and $\delta$ defining the angular position of the pixel on the focal plane that detects the feature. Assuming the sensor is chasing the target and adopting the conventional LVLH frame in which "x" defines the radial coordinate, "y" is along-track, and "z" is cross-track, the conversion to LVLH is given by

$$x = \rho \cos(\alpha) \cos(\delta) \tag{12}$$

$$y = \rho \sin(\alpha) \cos(\delta) \tag{13}$$

$$z = \rho \sin(\delta) \tag{14}$$

The covariance $R$ in sensor LVLH is computed by considering errors in $\rho, \alpha, \delta$, and then computing expected values of the errors in $x, y, z$. Employing the small angle approximation and neglecting quadratic and higher order error terms produces

$$R = \begin{bmatrix} \rho^2\sigma_\alpha^2 + \alpha^2\sigma_\rho^2 & \rho^2\alpha\sigma_\alpha^2 + \alpha\sigma_\rho^2 & \alpha\delta\sigma_\rho^2 \\ \rho^2\alpha\sigma_\alpha^2 + \alpha\sigma_\rho^2 & \sigma_\rho^2 + \rho^2\alpha^2\sigma_\alpha^2 + \rho^2\delta^2\sigma_\delta^2 & \rho^2\delta\sigma_\delta^2 + \delta\sigma_\rho^2 \\ \alpha\delta\sigma_\rho^2 & \rho^2\delta\sigma_\delta^2 + \delta\sigma_\rho^2 & \rho^2\sigma_\delta^2 + \delta^2\sigma_\rho^2 \end{bmatrix} \tag{15}$$

where the angles are in radians. Where required to put a range or angle value, the corresponding values measured for each feature should be used, producing a different $R$ matrix for each point. For simplicity, this paper uses the maximum measured range and angles for the edge of the focal plane for all feature points, allowing the same $R$ to be replicated in a block diagonal matrix for Eqs. (9)-(10) This should produce a measurement covariance that is conservative.

OLTAE produces a least squares fit for a single instance in time, in the dynamics simulation below an extended Kalman Filter (EKF) is used to filter the OLTAE output and estimate the relative pose through time. Thus, the output OLTAE state and covariance become the input measurement and measurement noise covariance for the EKF. It is assumed that 10 flashes from the LIDAR are processed in each OLTAE solution spanning 1 second, and thus measurements are processed in the EKF at 1 Hz.

### B. Pose Estimation Simulation

The simulation involves a sensor and target spacecraft in a lead-follower formation, in which the chasing sensor spacecraft is approaching the target. The translational dynamics are given by the linear CW equations[8]

$$\ddot{x} = 2n\dot{y} + 3n^2 x + u_x \tag{16}$$

$$\ddot{y} = -2n\dot{x} + u_y \tag{17}$$

$$\ddot{z} = -n^2 z + u_z \tag{18}$$

where $n$ is the mean motion of the target spacecraft and $u_i$ are the accelerations in each direction. The attitude dynamics are given by[8]

$$\dot{\boldsymbol{g}} = \frac{1}{2}[I + \tilde{\boldsymbol{g}} + \boldsymbol{g}\boldsymbol{g}^T]\boldsymbol{\omega} \tag{19}$$

$$\dot{\omega}_1 = \frac{I_2 - I_3}{I_1}\omega_2\omega_3 \tag{20}$$

$$\dot{\omega}_2 = \frac{I_3 - I_1}{I_2}\omega_1\omega_3 \tag{21}$$

$$\dot{\omega}_3 = \frac{I_1 - I_2}{I_3}\omega_2\omega_1 \tag{22}$$

$$\tag{23}$$

where $I$ are the principal moments of inertia of the body. In this simulation, we assumed torque-free attitude motion.

The features selected for this work are the corners of the shape model. These features are shown as black dots in Fig. 9, which shows examples of the flash LIDAR image of the target satellite rotated 45° around each of the body axes. These images show the flash LIDAR in the sensor focal plane, which is rotated with respect to the LVLH frame by 90° as illustrated in Fig. 10.

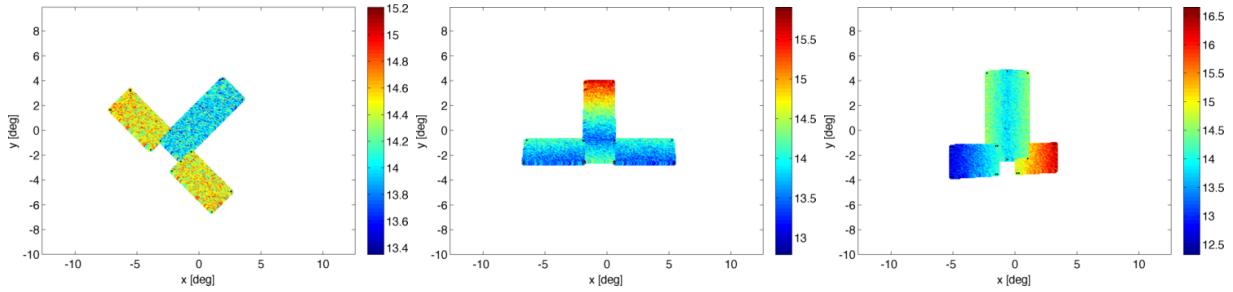


**Figure 9. Example flash LIDAR images of the target satellite.**

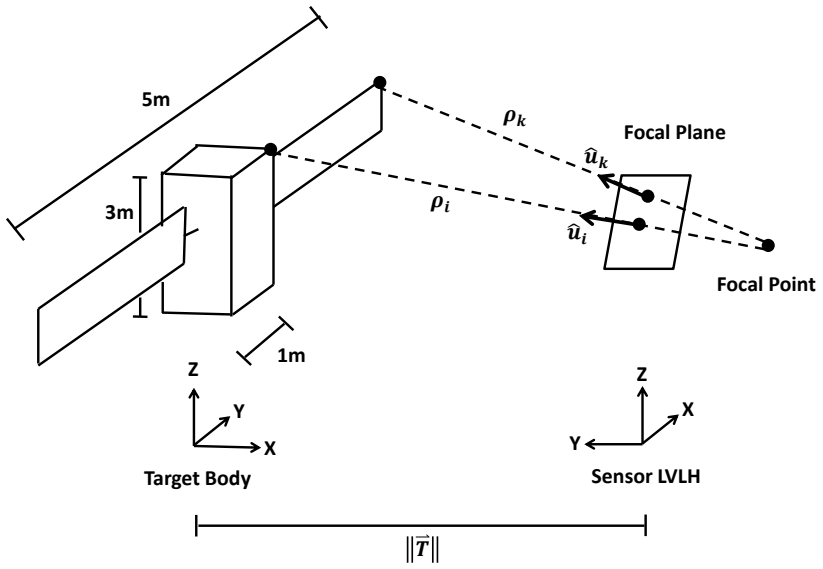


**Figure 10. Cartoon illustrating the sensor frame used in the simulations.**

It turns out that the issues with the measurement noise are more complicated due to the use of OLTAE to initially process the flash LIDAR measurements of the features. Three examples of OLTAE data are

shown in Figs. 11 - 13. In each figure, the errors in the Gibbs vector and the relative position for 10 data points at one time processed by OLTAE are shown along with the associated $3\sigma$ bounds computed by Eq. (10). In Fig. 11, the noise on the angle measurements was $\sigma_\alpha = \sigma_\delta = 1$ pixel (1 pixel = 0.00136 radians). Clearly in this case OLTAE underestimates the influence of noise in the measurements. Fig. 12 shows the same results with $\sigma_\alpha = \sigma_\delta = 5$ pixels. In this case, the covariances are more appropriate in that they encompass the errors. Finally, Fig. 13 shows the errors when the measurements were generated as 3-D vector measurements directly with $\sigma_y = 20$ cm and $\sigma_x = \sigma_z = 2$ cm (where $x$, $y$, and $z$ correspond to sensor LVLH frame coordinates - the same as the dynamics). In this case the covariances look appropriate to the errors in the data.

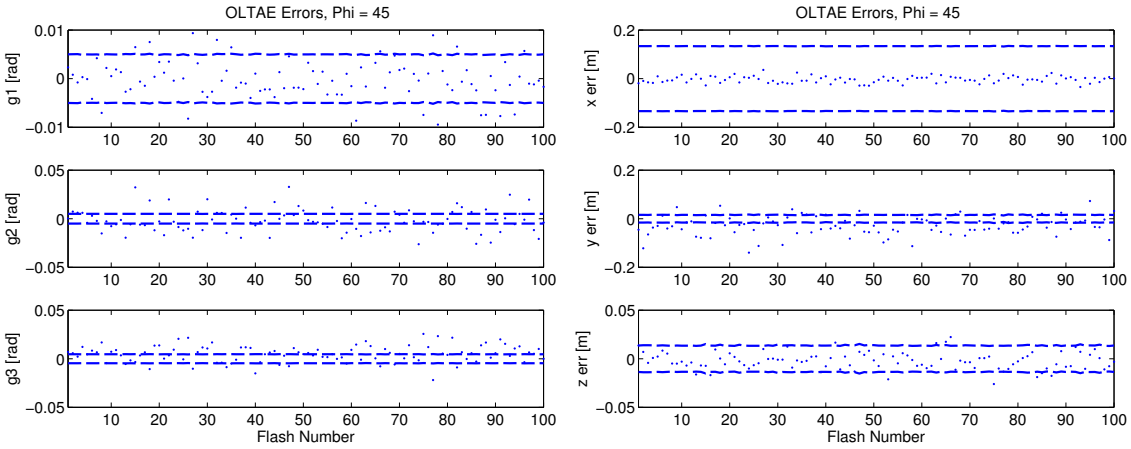


**Figure 11. OLTAE example errors for the Gibbs vector and relative position vector with 1 pixel angle noise.**

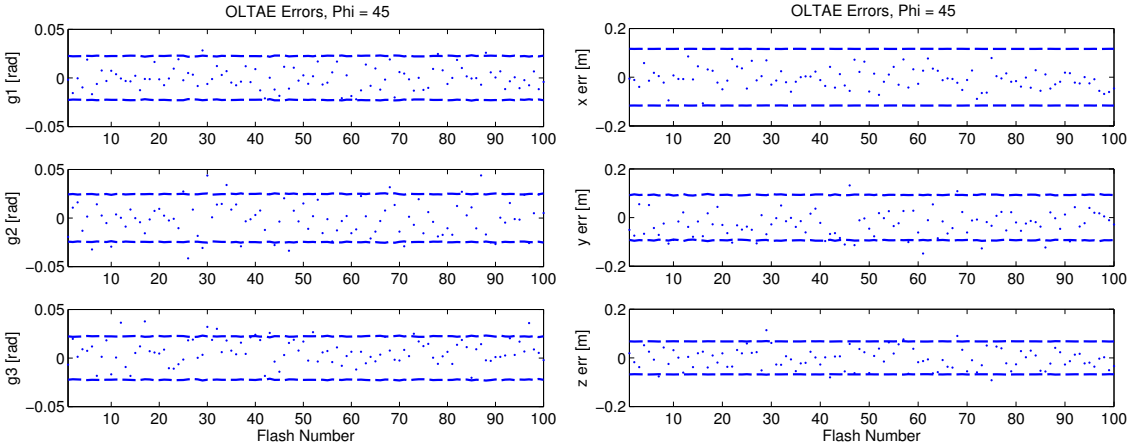


**Figure 12. OLTAE example errors for the Gibbs vector and relative position vector with 5 pixel angle noise.**

The summary of this is that there is a clear influence from the non-linearities present in this problem when using range and angle data from the flash LIDAR. These non-linearities become more significant with smaller angular noise. Thus, the result given Eq. (15) should be expanded to include higher order terms. Furthermore, the derivation above assumes that the measurements are made as 3-D vectors, so that the $H$ matrix is exact. However when the measurements are actually ranges and angles, this non-linearity can create inaccuracies.

The next step is to integrate the OLTAE processing of measurements with an EKF to estimate the full 6-dimensional pose including the dynamics between measurements. The model used in this study combines 10 flash images at a time through OLTAE, which produces an estimate of $\hat{\mathbf{g}}$ and $\hat{\mathbf{T}}$ once per second; these 1 Hz measurements are then fed to the EKF along with the associated covariance computed from OLTAE. The trajectory starts 20 m from the target satellite and closes to 5 m over 90 seconds. The target satellite is

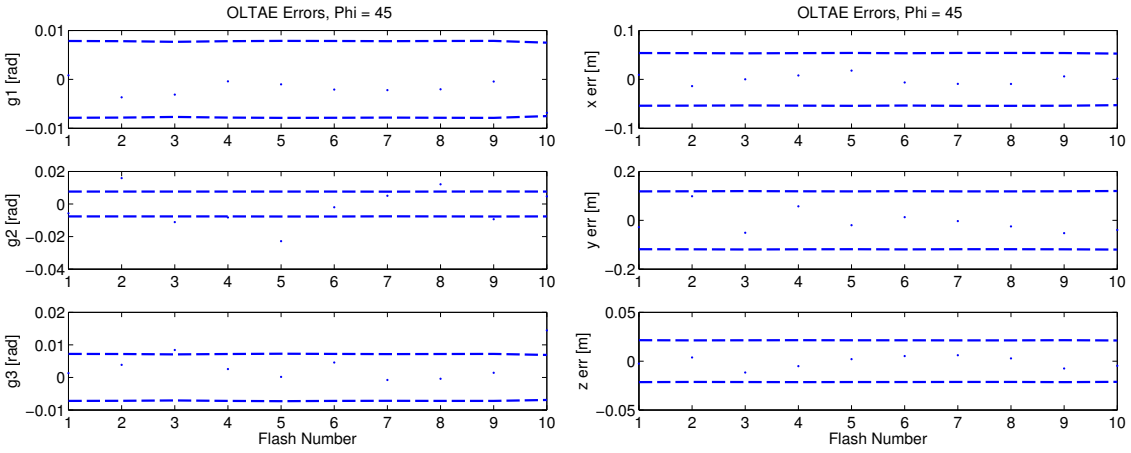


**Figure 13. OLTAE example errors for the Gibbs vector and relative position vector with 3-D vector measurements.**

spinning at 1 deg/sec, so that it spins 90° over the duration of this simulation. The initial relative attitude has the short edge of one of the target satellite solar arrays pointed at the sensor. We run three cases and compare their results below.

In the first case, the target satellite is spinning about the z-axis (the orbit normal direction), similar to the right-most example in Fig. 9. In this case, the range noise for each pixel is set at 20 cm, which corresponds to 1% of the initial 20 m separation distance. The estimate of the relative translation states are shown in Fig. 14 while the attitude states are shown in Fig. 15. While this case performs very well in general, close inspection of the end of the time shows that the state estimates are starting to diverge. In particular, the third component of the Gibbs vector has already drifted outside of the $3\sigma$ covariance bounds. This is due to the fact that as the target approaches a 90° spin, the solar panels become face on to the sensor, and the range component of the measurements becomes more useful for accurately estimating the attitude. It turns out that the 20 cm range noise added here means that the sensor can only estimate down to approximately ±5° around the face on attitude, thus the estimate becomes more uncertain here. The effect of this decrease in knowledge can be seen more clearly by looking at the spin angle estimate errors in Fig. 16, where it is clear that the estimate is losing accuracy at this attitude.

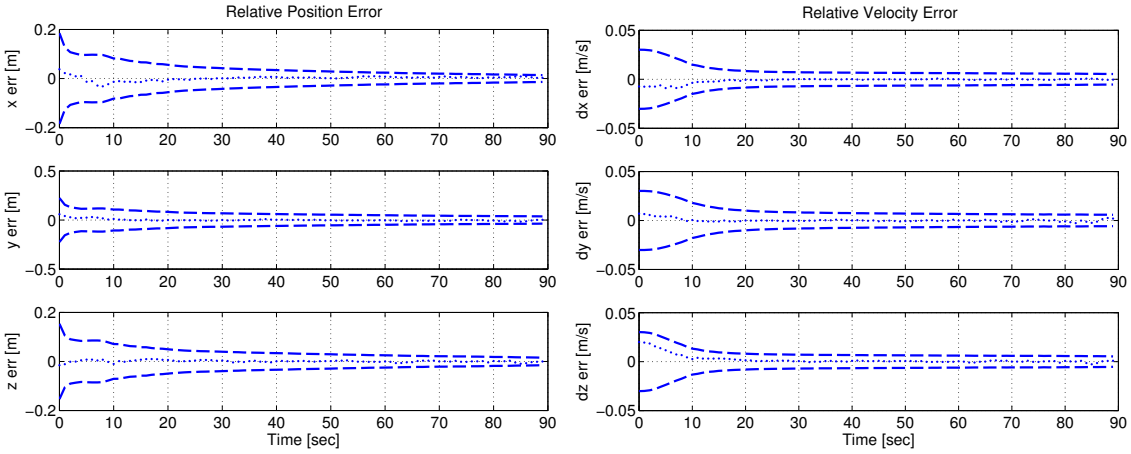


**Figure 14. EKF relative position (left) and velocity (right) estimation errors and $3\sigma$ covariances for case with 20 cm range noise spinning about the z-axis.**

In our discussions with Ball Aerospace about the accuracy of the flash LIDAR range measurements, it was indicated that the accuracy at short ranges (approximately $< 100$ m), the range accuracy bottoms out around 1 cm. Therefore, in this case, the same situation as the previous case is run except that the range

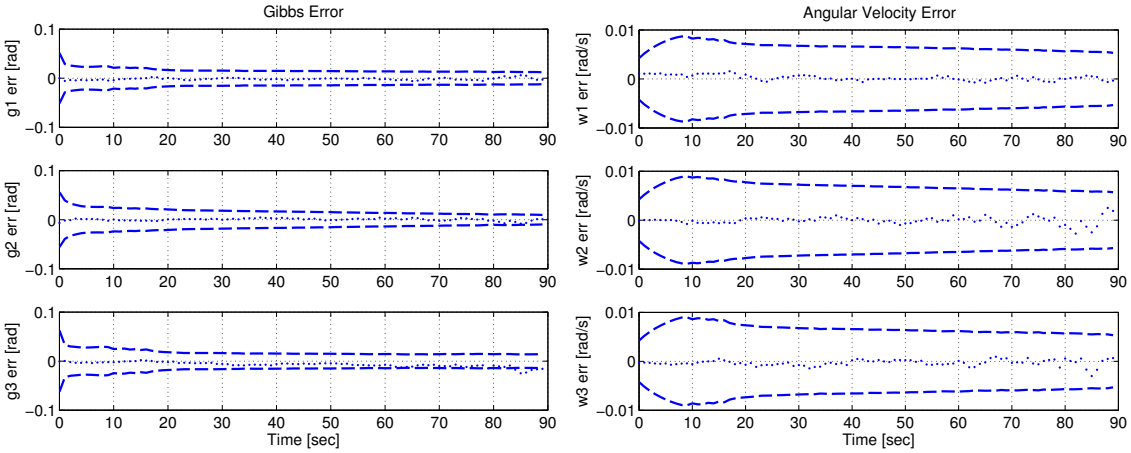


**Figure 15. EKF Gibbs vector (left) and angular velocity (right) estimation errors and $3\sigma$ covariances for case with 20 cm range noise spinning about the z-axis.**

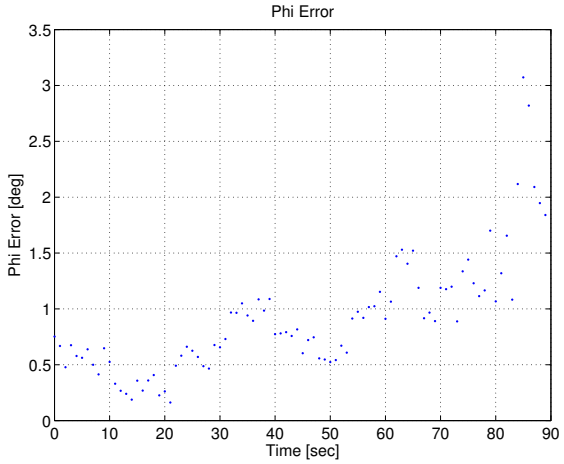


**Figure 16. EKF spin angle estimation errors for case with 20 cm range noise spinning about the z-axis.**

noise is tightened down to 1 cm. Note the erroneous initial conditions are also different in this case as they are randomly generated. As expected, the improvement in range noise allows for more accurate observability of the attitude when the target is face on, as can be seen in Figs. 17 - 19.

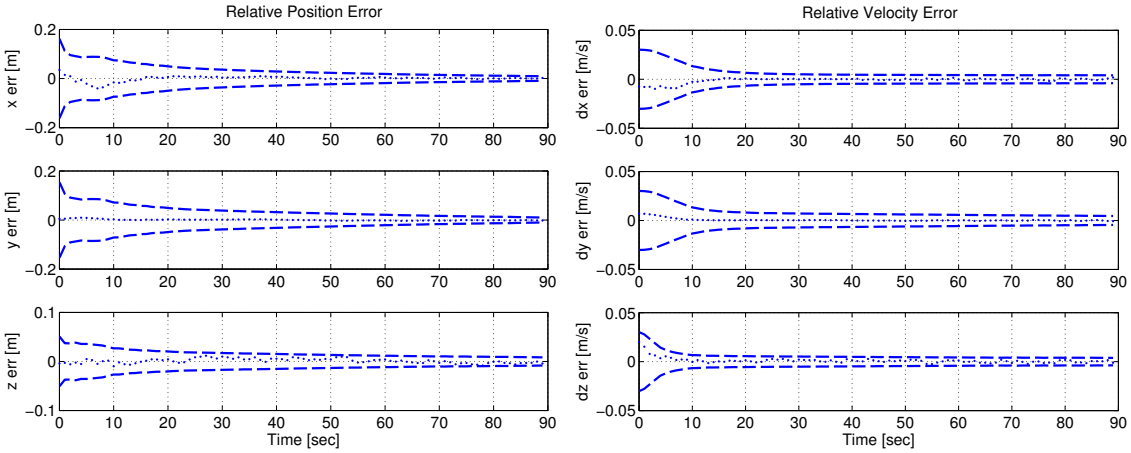


**Figure 17. EKF relative position (left) and velocity (right) estimation errors and $3\sigma$ covariances for case with 1 cm range noise spinning about the z-axis.**

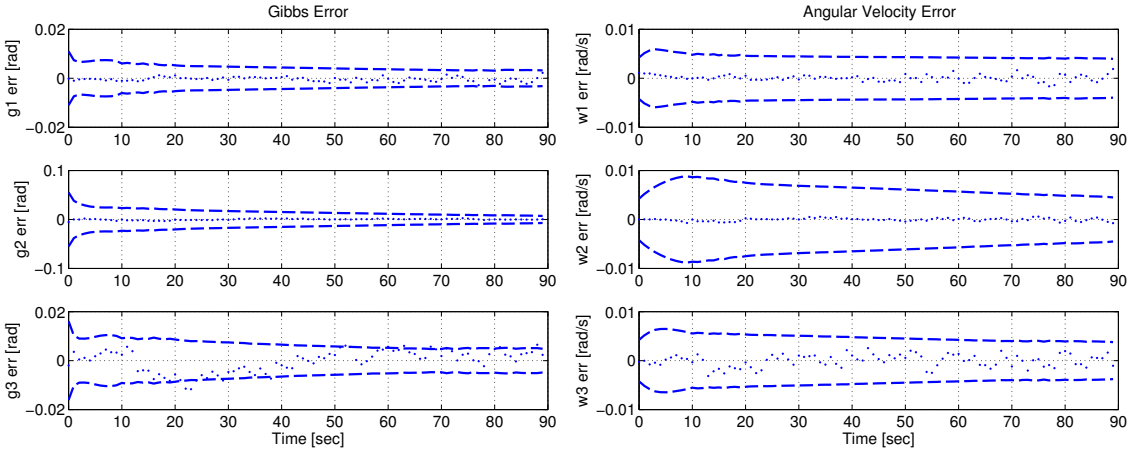


**Figure 18. EKF Gibbs vector (left) and angular velocity (right) estimation errors and $3\sigma$ covariances for case with 1 cm range noise spinning about the z-axis.**

Finally, to ensure that the filter performance worked for a more general case, we ran a third case with a randomly chosen spin axis for the target satellite, as opposed to the body fixed z axis, which is an axis of symmetry for the target shape. This case also used 1 cm range noise. Again, the results show very good accuracy of the pose is obtained during this simulation. The results are illustrated in Figs. 20 - 22.

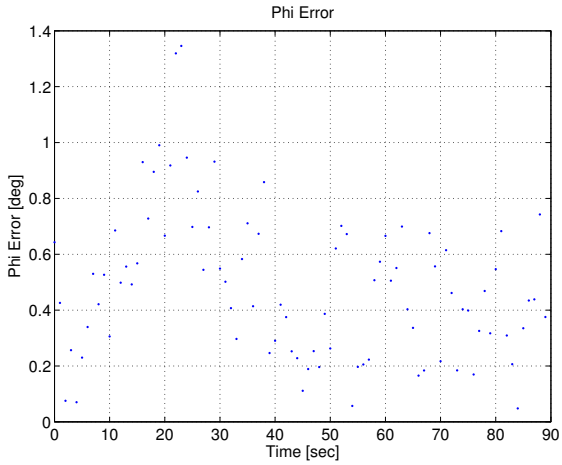


**Figure 19. EKF spin angle estimation errors for case with 1 cm range noise spinning about the z-axis.**

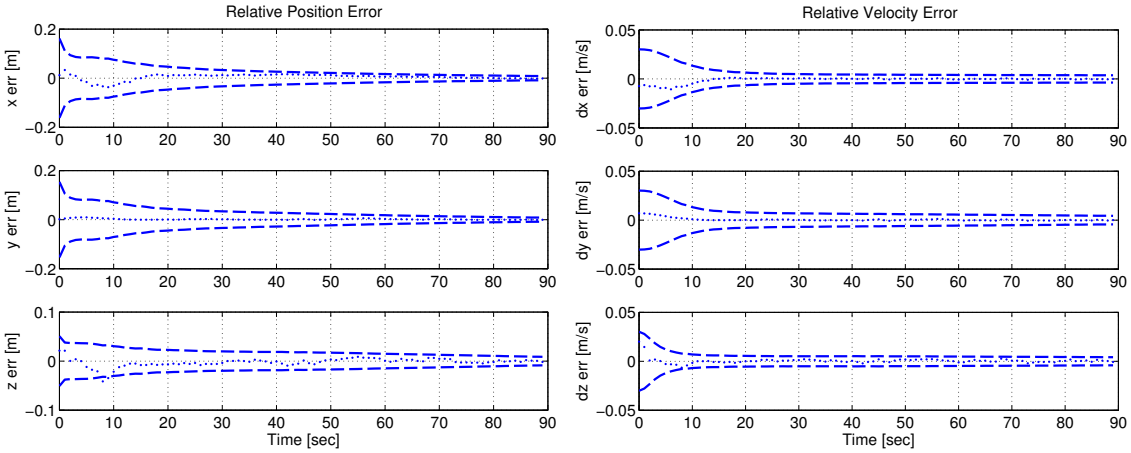


**Figure 20. EKF relative position (left) and velocity (right) estimation errors and $3\sigma$ covariances for case with 1 cm range noise and a random spin axis.**

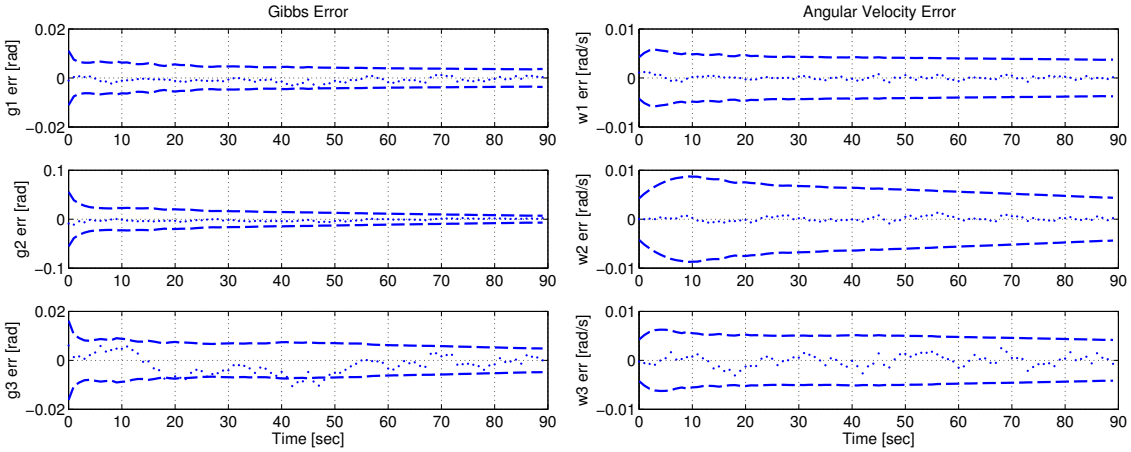


**Figure 21. EKF Gibbs vector (left) and angular velocity (right) estimation errors and $3\sigma$ covariances for case with 1 cm range noise and a random spin axis.**

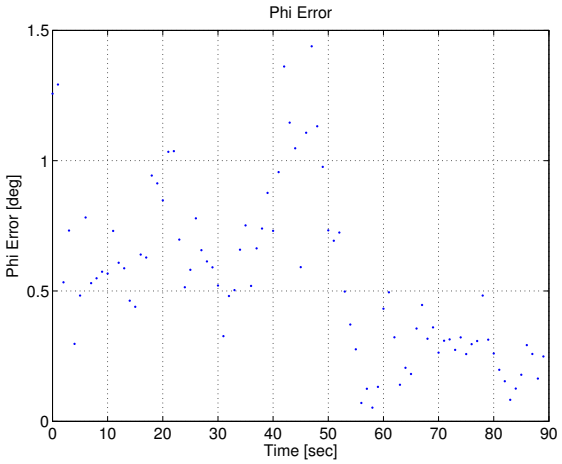


**Figure 22. EKF spin angle estimation errors for case with 1 cm range noise and a random spin axis.**

## IV. Conclusion

In this paper, the initial results of a study using flash LIDAR for relative pose and trajectory estimation are presented. The analysis is presented in two parts. First, the approach navigation using a flash LIDAR was analyzed where no information is assumed about the target body, and the flash data is processed as one averaged centroid measurement. Very good relative navigation accuracy can be achieved, with errors governed by the size of the target body. Furthermore it is shown that the errors are small enough and that their growth is slow enough to allow for time to recover in case of sensor malfunctions or other issues on the way to rendezvous. The second piece of analysis combined the OLTAE algorithm with an EKF to simultaneously estimate the relative trajectory and pose. Again, the extreme accuracy of the flash LIDAR can provide very good relative solutions if the shape model is known as assumed here.

There is extensive future work to be done in this area. Most importantly, we will obtain data to implement and develop methods to build shape models, identify features, and to quickly process the data for on-board use. This will surely inform more detailed measurement and error models which can be used to improve the fidelity of simulations like those presented here. Furthermore, we intend to study the impact of approach trajectory on relative state observability.

## V. Acknowledgments

The authors gratefully acknowledge support from the FAA Center of Excellence in Commercial Space Transportation.

## References

[1]D'Souza, C., et al., "Orion Rendezvous, Proximity Operations, and Docking Design and Analysis," AIAA Guidance, Navigation, and Control Conference, Hilton Head, SC, 2007, Paper No. AIAA 2007-6683

[2]Rohrschneider, R. and Tandy, W., "Pose Determination Using Only 3D Range Images from the STORRM Mission," 36th ANNUAL AAS GUIDANCE AND CONTROL CONFERENCE, Breckenridge, CO, 2013, Paper No. AAS 13-104

[3]K. Shahid and G. Okouneva, "Intelligent LIDAR Scanning Region Selection for Satellite Pose Estimation, Computer Vision and Image Understanding, Vol. 107, February 2007, pp. 203209.

[4]Christian, J., Patangan, M., Hinkel, H., Chevray, K., Brazzel, J., "Comparison of Orion Vision Navigation Sensor Performance from STS-134 and the Space Operations Simulation Center," Proceedings of the AIAA Guidance, Navigation, and Control Meeting, Minneapolis, MN, 2012, pp. 118, Paper No. AIAA 2012-5035

[5]D. G. Lowe, "Distinctive Image Features From Scale Invariant Keypoints, International Journal of Computer Vision, Vol. 60, No. 2, 2004, pp. 91110.

[6]B. Flewelling, "3D Multi-Field Multi-Scale Features From Range Data in Spacecraft Proximity Operations". PhD thesis, Texas A&M University, College Station, TX, 2012.

[7]D. Mortari, J. Rojas, and J. Junkins, "Attitude and Position Estimation from Vector Observations, Proceedings of the AAS Space Flight Mechanics Meeting, Maui, HI, 2004, pp. 118.

[8]Schaub, H. P. and Junkins, J. L., Analytical Mechanics of Space Systems, 2nd Edition, AIAA Education Series, AIAA, Inc., Reston, VA, 2009.

[9]Majji, Manoranjan, et al. "Registration of LiDAR point clouds using image features." Proc., ASPRS 2010 Annual Conf. 2010.

[10]MORTARI, D., MARKLEY, FL, and JUNKINS, JL Optimal Linear Attitude Estimator, Advances in the Astronautical Sciences, Vol. 105, Pt. I, 2000.